BIOCHEMISTRY
including biophysical chemistry & molecular biology

Article

pubs.acs.org/biochemistry

Engineering the Organophosphorus Acid Anhydrolase Enzyme for Increased Catalytic Efficiency and Broadened Stereospecificity on Russian VX

Courtney M. Daczkowski,[†] Scott D. Pegan,[*,†,‡] and Steven P. Harvey[*,§]

[†]Department of Pharmaceutical and Biomedical Sciences, University of Georgia, Athens, Georgia 30602, United States
[‡]U.S. Army Reserve 377th Sustainment Command Detachment 8, Aberdeen Proving Ground, Maryland 21010-5424, United States
[§]U.S. Army Edgewood Chemical Biological Center, Aberdeen Proving Ground, Maryland 21010-5424, United States

Supporting Information

ABSTRACT: The enzyme organophosphorus acid anhydrolase (OPAA), from *Alteromonas* sp. JD6.5, has been shown to rapidly catalyze the hydrolysis of a number of toxic organophosphorus compounds, including several G-type chemical nerve agents. The enzyme was cloned into *Escherichia coli* and can be produced up to approximately 50% of cellular protein. There have been no previous reports of OPAA activity on VR {Russian VX, *O*-isobutyl *S*-[2-(diethylamino)ethyl] methylphosphonothioate}, and our studies reported here show that wild-type OPAA has poor catalytic efficacy toward VR. However, via application of a structurally aided protein engineering approach, significant improvements in catalytic efficiency were realized via optimization of the small pocket within the OPAA's substrate-binding site. This optimization involved alterations at only three amino acid sites resulting in a 30-fold increase in catalytic efficiency toward racemic VR, with a strong stereospecificity toward the P(+) enantiomer. X-ray structures of this mutant as well as one of its predecessors provide potential structural rationales for their effect on the OPAA active site. Additionally, a fourth mutation at a site near the small pocket was found to relax the stereospecificity of the OPAA enzyme. Thus, it allows the altered enzyme to effectively process both VR enantiomers and should be a useful genetic background in which to seek further improvements in OPAA VR activity.

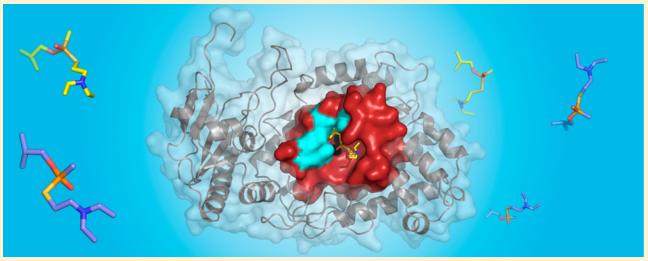

The potential threat of an intentional release of chemical nerve agents along with thousands of fatalities in developing countries every year caused by pesticide poisoning has made treatments for these types of poisonings a persistent focus for therapeutic intervention.[1,2] Current treatments for nerve agent poisoning involve a combination of atropine (a muscarinic antagonist), pralidoxime (also known as 2-PAM, a reactivator of poisoned acetylcholinesterase enzymes), and benzodiazepines to control seizures.[3]

Intriguingly, another method of treating organophosphate poisoning has recently emerged through the potential use of catalytic enzymes to detoxify these poisons in the blood. In detail, this approach offers the particular advantage of hydrolyzing organophosphates before they enter the tissue where they bind acetylcholinesterase in the neuromuscular junctions. Therefore, such enzymes can at a minimum work in a complementary manner to, and in concert with, current treatments to improve survival rates. This was demonstrated when a liposome-encapsulated diisopropylfluorophosphate (DFP)-hydrolyzing enzyme, known as an organophosphorus acid anhydrolase (OPAA), was used in conjunction with atropine and 2-PAM to confer 25 LD_{50}s of protection against diisopropylfluorophosphate.[4]

OPAA (EC 3.1.8.2) is one example of a larger class of enzymes known as phosphotriesterases, initially identified more than 60 years ago and generally recognized for their ability to detoxify organophosphates.[9] Phosphotriesterase (PTE), methyl parathion hydrolase (MPH), diisopropylfluorophosphatase (DFP), and paraoxonase 1 (PON1) are the other examples from this class.[5] These enzymes are all hydrolases with hydrophobic active sites and a requirement for divalent metals, but they differ in terms of sequence, structure, and their catalytic mechanisms. The native activity of OPAA is that of a prolidase.[6]

The OPAA enzyme from the Gram-negative, aerobic, short rod bacterium *Alteromonas* sp. JD6.5 has drawn particular focus because it has very high activity on GD as well as a very high level of expression in *Escherichia coli*.[7,8] However, it has not been reported to have any activity against V-type nerve agents, and to the best of our knowledge, there have been no previous reports of its engineering. An effective broad-spectrum enzymatic antidote addressing nerve agent poisoning would need to include enzymes with good catalytic efficiency (target

Received: June 5, 2015
Revised: August 31, 2015
Published: September 29, 2015

DOI: 10.1021/acs.biochem.5b00624
Biochemistry 2015, 54, 6423−6433

value of ~10^7 min^{-1} M^{-1}) on as many relevant substrates as possible. Regrettably, the activity of the wild-type OPAA enzyme on VR (approximately 5×10^2 M^{-1} min^{-1}) falls well short of what is necessary for use in that capacity. However, unlike those of all other OPAAs, the atomic level structure of the OPAA from bacterium *Alteromonas* sp. JD6.5 is known. Although density for only 440 of 517 amino acids was observed, truncation of the last 77 amino acids has been shown not to affect enzymatic activity.[11] As a result, the OPAA structure provides an initial platform for a structurally guided protein engineering approach to the improvement of OPAA's catalytic activity toward organophosphates. Therefore, this study uses a 440-amino acid variant of OPAA from *Alteromonas* sp. JD6.5 as a starting point to greatly increase the activity of OPAA on VR via structurally guided mutagenesis.

With enzyme−substrate interactions more often than not being very stereospecific, enhancing the catalytic activity of OPAA may only be one component necessary to achieve an effective catalytic antidote. Previous reports have shown that the toxicity of chemical nerve agents can be extremely stereospecific, as evidenced by the case of soman, where the most toxic C(−)P(−) or S_CS_P enantiomer is >100 times more toxic than the least toxic C(+)P(+) or R_CR_P enantiomer, corresponding to mouse LD_{50} values of 38 and >5000 μg/kg, respectively.[9]

Understandably, an effective enzymatic, broad-spectrum antidote to nerve agent poisoning would need to include enzymes (possibly a cocktail of enzymes) that possess not only good catalytic efficiency on racemic materials, but activity specifically directed toward the more toxic enantiomers of all relevant substrates. This combination of catalytic efficiency coupled with the proper stereochemistry was achieved recently with the H257Y/L303T mutant of the bacterial phosphotriesterase (PTE) enzyme for G-agent substrates.[10] The mutant enzyme possessed catalytic efficiencies approximately 10 times greater than that of wild-type PTE on sarin and cyclosarin and approximately 100 times greater on soman, as well as a reversal of stereospecificity so that the mutant possessed greater activity on the more toxic P(−) or S_P enantiomer than the P(+) or R_P enantiomer of cyclosarin, representing a reversal of the wild-type enzyme's preference.

VX {*O*-ethyl *S*-[2-(diisopropylamino)ethyl] methylphosphonothioate}, which is a structural isomer of VR, has an ~13-fold difference in toxicity between its enantiomers, with the P(−) or S_P enantiomer being the more toxic of the two,[11] although considering the extreme toxicity of the racemic material, both enantiomers would clearly require treatment. Given that VX and VR are structural isomers and have similar racemic toxicities[9,11] and trends in cholinesterase inhibition constants for the respective enantiomers [the P(−) enantiomers of each are much more inhibitory],[16] and that both are treated with similar modalities using acetylcholinesterase reactivators,[12] it is likely that the relative toxicity of their respective enantiomers follows a similar pattern. Therefore, we sought to identify mutations that would increase the catalytic efficiency and broaden the stereospecificity of OPAA to allow catalysis on both enantiomers of VR.

Through modification of the small pocket within the OPAA substrate-binding site, an enzyme possessing a >30-fold increase in catalytic efficiency on racemic VR has been realized. In detail, catalytic efficiency was increased through three successive amino acid changes in the active site that caused both an increase in specific activity and a decrease in the K_m. Subsequent alteration of a fourth amino acid decreased the racemic catalytic efficiency approximately 2-fold but, more importantly, relaxed the stereospecificity allowing the mutant enzyme to catalyze both enantiomers of VR with similar efficiencies.

EXPERIMENTAL PROCEDURES

Materials. Chemical agent substrates were obtained from Edgewood Chemical Biological Center stocks and were Chemical Agent Standard Analytical Reference Materials, typically >95% pure. Chemicals, biochemicals, buffers, and solvents were purchased from Sigma-Aldrich Chemical Co. (St. Louis, MO), Fisher Scientific, Inc. (Pittsburgh, PA), or Acros Organic (Morris Plains, NJ), unless otherwise indicated. 5,5′-Dithiobis(2-nitrobenzoic acid) (DTNB, CAS Registry No. 69-78-3) was purchased from Sigma (item number D8130, lot number 54H0479). Ethyl acetate (CAS Registry No. 141-78-6) was purchased from Aldrich (item number 11,0002-7, lot number 143110BZ). Bis-tris-propane (CAS Registry No. 66431-96-5) was purchased from Sigma (item number B6755-1KG, lot number SLBD7878V). $MnCl_2$ (CAS Registry No. 13446-34-9) was purchased from Sigma (item number M-3634-100G, lot number 111 K0151).

OPAA Expression Vector and Site-Directed Mutagenesis of the OPAA Gene. The gene encoding the OPAA enzyme was originally cloned from *Alteromonas* sp. JD6.5, as described previously.[13] The OPAA gene utilized is a naturally occurring variant. It differs from previous OPAA entry Q44238.3 by three amino acids at sites 210, 211, and 314. The present gene, which we modified by site-directed mutagenesis, lacks the last 77 carboxyl-terminal amino acids of the OPAA enzyme. This truncated gene was cloned into the *Nco*I and *Eco*RI sites of the pSE420 expression vector of *E. coli*. The resulting mutant plasmids were introduced into *E. coli* BL21(DE3) competent cells by electroporation and were typically grown to late log phase in 1 L flasks without induction to produce enzyme. The complete coding regions for all mutant enzymes were sequenced by DNA2.0 (www.dna20.com).

Production and Purification of Engineered OPAAs. The engineered OPAA enzymes were prepared by a method similar to that described previously for OPAA.[13] Briefly, the cells were harvested and centrifuged, and the proteins from the supernatant were precipitated in 65% ammonium sulfate. This pellet was resuspended in 13 mL of 10 mM bis-tris-propane (pH 8.0) with 0.1 mM $MnCl_2$ and passed through a size exclusion column. The active fractions were pooled and loaded on a 10 mL Q Sepharose column and eluted with a 0.2 to 0.6 M NaCl gradient. The active fractions from the Q-Sepharose column were pooled, precipitated in 65% ammonium sulfate, and resuspended in and dialyzed against 10 mM bis-tris-propane (pH 8.0) with 0.1 mM $MnCl_2$. The resulting protein migrated with apparent homogeneity via sodium dodecyl sulfate−polyacrylamide gel electrophoresis.

VR Enzymatic Assays. The kinetic constants were determined by spectrophotometry using 0.3 mM DTNB in 50 mM bis-tris-propane buffer (pH 8.0) and 0.1 mM $MnCl_2$ at 25 °C in a 1 mL cuvette with a total sample volume of 0.5 mL. Reactions were monitored spectrophotometrically at 412 nm typically for 5 min, and activity was calculated using an extinction coefficient of 14150 M^{-1} cm^{-1}. The assay measured the concentration of free thiol from the enzyme-catalyzed cleavage of the P−S bond of VR.

DOI: 10.1021/acs.biochem.5b00624
Biochemistry 2015, 54, 6423−6433

Kinetic parameters were calculated using Biosoft EnzFitter (Biosoft.com). Activity data were generally collected at substrate concentrations ranging from $^1/_3$ to 3 times the K_m under conditions that consumed <10% of the substrate. At least five different substrate concentrations were used for each determination.

Single-enantiomer isolates for polarimetry were prepared from a 900 mL solution of 50 mM bis-tris-propane buffer (pH 8.0) containing 0.5 mM substrate. To facilitate rapid dissolution, the substrates were diluted into 1 mL of isopropyl alcohol prior to addition to the buffer. The solution was brought to 35 °C, and the reaction was initiated with the addition of 0.93 μg/mL enzyme. Reaction progress was monitored spectrophotometrically, and when the product concentration had just exceeded the remaining VR concentration (i.e., the point at which the preferred enantiomer would be essentially completely hydrolyzed), the reaction was stopped by plunging the mixture into a slushy ice bath and extracting twice with 50 mL of ethyl acetate, shaking vigorously each time. The organic layer was removed, concentrated to approximately 1 mL by rotary evaporation, and used for polarimetry in an Anton Paar MCP 500 instrument.

Crystallization of Engineered OPAAs. Initial crystal conditions for OPAA Y212F were determined from high-throughput screening of Qiagen Nextel Screens, Classics, Classics II, PEGs, PEGs II, Anion, Cation, PhClear I, and PhClear II suites, in a 96-well hanging drop format using a TTP Mosquito Crystal liquid handling robot. Drops contained 150 nL of the protein solution to 150 nL of the precipitate solution. The reservoir volume was 100 μL. Initial screening resulted in crystals from conditions with 10% PEG 4000, 20% 2-propanol, and 8.5 mg/mL OPAA Y212F. However, utilizing a gradient screen of PEG 4000 and 2-propanol screening precipitant conditions containing 4% PEG 4000 and 20% 2-propanol produced the most viable crystals. These crystals were optimized using the Additive HT Screen from Hampton Research.

X-ray Structure of Engineered OPAAs. X-ray data sets were collected using crystals mounted onto polymer loops (Mitegen) and flash-cooled in liquid nitrogen. All crystals were passed through a cryopreservation solution of 20% 2-propanol, 15% PEG 4000, and 5% glycerol before being mounted under a stream of dry N_2 at 100 K. All data were collected at a wavelength of 1 Å. For OPAA Y212F, the 2.1 Å data set was collected using SER-CAT beamline 22-BM and a MAR 225 detector. For OPAA Y212F in complex with mipafox and OPAA FLY, the 2.4 Å data sets were collected using SER-CAT beamline 22-ID and a MAR300hs detector.

X-ray images were indexed, processed, integrated, and scaled using HKL2000.[14] An initial phase solution for OPAA Y212F was elucidated using wild-type OPAA [Protein Data Bank (PDB) entry 3L24] as a starting model for molecular replacement using Phaser.[15] Initial structures for OPAA Y212F with mipafox bound and OPAA FLY were found using the OPAA Y212F structure as a search model. All structures were subjected to Phenix autobuild in which water molecules were initially added. Subsequent refinement utilized iterative cycles of model building and refinement using COOT and Phenix Refine, respectively.[16,17] Water molecules were added and deleted using the check water application in COOT before being individually examined. The final model was checked for structural quality using the Molprobity and other Phenix suite validation programs. The data refinement statistics are listed in Table 1.

Table 1. Genotypes and Kinetic Parameters of Purified OPAA Enzymes

enzyme	genotype	k_{cat} (min^{-1})	K_m (μM)	k_{cat}/K_m (M^{-1} min^{-1})
WT	wild-type	1.8 ± 0.12	3280 ± 551	548 ± 128
F	Y212F	11 ± 0.75	4482 ± 680	2451 ± 540
FL	Y212F/V342L	21 ± 1.1	1767 ± 258	11894 ± 2349
FLY	Y212F/V342L/I215Y	38 ± 2.7	1915 ± 456	19642 ± 6071
FLYD	Y212F/V342L/I215Y/H343D	18 ± 1.3	2075 ± 460	8890 ± 258

RESULTS

Enhancing the OPAA Enzymatic Activity for the VR Chemical Agent through the Introduction of Site-Specific Mutations. Kinetic analysis of the wild-type enzyme on VR showed a k_{cat}/K_m value of approximately 2.48×10^2 M^{-1} min^{-1}, a rate probably 4 orders of magnitude too slow to be effective as a medical countermeasure (Table 1). The OPAA substrate-binding site is composed of a small pocket, a large pocket, and a leaving group pocket. The large pocket is formed by Leu225, His226, His332, and Arg418. The leaving group pocket is composed of Tyr292 and Leu366. The small pocket is formed by residues Tyr212, Val342, His343, and Asp45 from the N-terminal domain of the opposite subunit in the dimer. All three pockets are in the proximity of the binuclear active site.

Attempts to increase the size of the leaving group site through mutation of Tyr292 proved to be unsuccessful. Twelve individual mutants (A, D, F, G, H, I, K, L, P, R, S, and V) were expressed and purified, but no significant increase in 3 mM VR activity was observed from substitution of any of these amino acids (Figure S2). This suggested that enlargement of the leading group to facilitate the larger VR molecule, as compared to GD, for instance, may not be a practical way forward toward increasing VR activity within OPAA.

As the larger pocket is already significantly large enough to accommodate the side chains of VR, the focus for optimization of OPAA was placed on the small pocket. Initially, Tyr212 was selected for mutagenesis as its ring system forms one of the small pocket walls. Subsequently, all amino acids except isoleucine were substituted into the Tyr212 site. Individual mutants were purified and assayed on 3 mM VR (Figure S2). Intriguingly, OPAAs containing the Y212F or Y212V substitution demonstrated a significant increase in activity toward 3 mM VR. As one of the more active mutants, OPAA Y212F underwent full kinetic analysis. Excitingly, its k_{cat} was 5 times higher than that of truncated wild-type OPAA, while its K_m remained largely unchanged. This translated into a catalytic efficiency roughly 5-fold higher than that of truncated wild-type OPAA (Table 1 and Figure 1).

To grasp how the nature of the active site may have changed by alteration of Tyr212 within the small pocket of the OPAA active site, OPAA Y212F was expressed, purified, and initially screened utilizing crystal conditions from full-length OPAA.[18] Regrettably, only frail crystals composed of thin plates were obtained after several rounds of optimization. As a result, OPAA Y212F was screened against several suites of commercially available precipitant screens followed by optimization via an additive screen. Final OPAA Y212F crystals

DOI: 10.1021/acs.biochem.5b00624
Biochemistry 2015, 54, 6423−6433

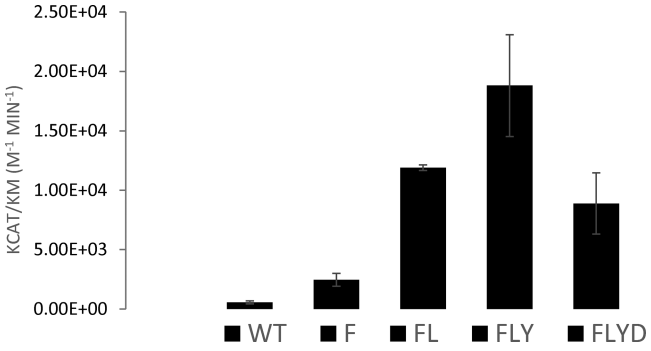

Figure 1. OPAA k_{cat}/K_m values for WT, F, FL, FLY, and FLYD. All values were measured spectrophotometrically at 25 °C and pH 8.0.

were obtained through hanging-drop vapor diffusion at 20 °C and included using a 500 μL reservoir with 2 μL hanging drops mixed 1:1 with protein solution and 0.25 μL of 0.1 M $BaCl_2$. A crystal from these conditions yielded a 2.1 Å data set in space group *C*2 (Table 2).

Table 2

	OPAA Y212	OPAA Y212 Mipafox	OPAA FLY
Data Collection			
space group	*C*2	*C*2	*C*2
unit cell dimensions			
a, *b*, *c* (Å)	103.4, 67.9, 140.5	104.5, 68.2, 142.5	102.9 68.8 139.4
α, *β*, *γ* (deg)	90.0, 110.1, 90.0	90.0, 110.5, 90.0	90, 109.6, 90
resolution (Å)	50.0−2.1	50.0−2.4	50.0−2.2
no. of reflections observed	182172	124112	209219
no. of unique reflections	49830	37080	46682
R_{merge} (%)[b]	7.5 (16.1)[a]	9.2 (44.2)[a]	8.3 (28.4)[a]
$I/\sigma I$	18.8 (11.0)[a]	10.7 (2.3)[a]	18.3 (3.1)[a]
completeness (%)	99.6 (99.9)[a]	98.5 (99.2)[a]	98.7 (82.8)
Refinement			
resolution range (Å)	32.9−2.11	48.9−2.4	48.5−2.2
no. of reflections in working set	49820	35090	46673
no. of reflections in test set	2526	1990	2355
R_{work} (%)[c]	17.2 (19.9)[a]	17.6 (22.5)[a]	16.2 (21.4)[a]
R_{free} (%)[c]	21.2 (19.0)[a]	22.6 (28.8)[a]	21.8 (27.8)[a]
root-mean-square deviation			
bond lengths (Å)	0.003	0.010	0.002
bond angles (deg)	0.6	0.96	0.63
no. of atoms (protein/water/ligand)	7002/712/23	6915/377/38	7064/470/19
average *B* factor (Å^2)			
total	29.8	39.2	45.3
protein	29.1	39	45.1
water	36.7	40.3	48.7
ligand	33.8	60.1	69.1

[a]Data for the last resolution shell are given in parentheses. [b]$R_{merge} = \sum_h\sum_i|I_i(h) - \langle I(h)\rangle|/\sum_h\sum_i I_i(h)$, where $I_i(h)$ is the *i*th measurement and $\langle I(h)\rangle$ is the weighted mean of all measurements of $I(h)$. [c]R_{work} and $R_{free} = h[|F(h)_{obs}| - |F(h)_{calc}|]/h|F(h)_{obs}|$ for reflections in the working and test sets, respectively.

Inspection of the OPAA Y212F active site revealed organization of the binuclear manganese(II) active site largely and surprisingly unchanged from the previous OPAA structure of PDB entry 3L24 (Figure 2). The substitution of OPAA Tyr212 with phenylalanine did remove the presence of a hydroxyl group, which formed the underpinning of an H-bonding network among Tyr212, Asp255, and Asp244 as well as with the amides of Gly246 and Ala245 within wild-type OPAA. Although the dynamics of the active site may have been altered through the loss of this bonding system, the phenylalanine substitution did not appear at first glance to drastically impact the binuclear metal organization and coordination within OPAA Y212F (Figure 2). As in its wild-type counterpart, additional density beyond the binuclear metal center was visualized within the OPAA Y212F active site. Specifically, considerable $F_o - F_c$ density within a simulated annealing omit map was observed that could not be accurately fit to any buffer, or crystallographic reagents, including the glycerol, contained in the cryogenic soaking solution. The bulk of this density did appear to be a shape and size match for glycolate, which has been previously reported to likely bind within the wild-type OPAA active site and supported by inhibition studies.[18] However, placement of the glycolate was slightly shifted from that observed in its wild-type counterpart and still left a significant $F_o - F_c$ peak between the two metals. This signal was only fully accounted for when a hydroxide ion was placed in it (Figure 2b). The resulting active site illustrates a mix of first-sphere metal bonds ranging from 1.8 to 2.2 Å and H-bonds ranging from 2.4 to 3.5 Å involving the glycolate, hydroxide ion, and coordinating aspartic acid and glutamate residues (Figure 2).

To reveal if any additional alterations may be visualized upon binding a substrate, the pesticide mipafox was cocrystallized with OPAA Y212F under the same conditions as the holo form of OPAA Y212F by using a final mipafox concentration of 790 μM. Prominent $F_o - F_c$ density within a simulated annealing omit map was observed within the active site. Refinement with mipafox, or its OPAA-facilitated product, *N*,*N*′-diisopropyldiamidophosphate (DDP), suggested the ligand within the active site was DDP (Figure 3a,b). Specifically, the bond distances and geometry formed by its diamidophosphate core within the unaccounted-for density are similar to those found in a wild-type counterpart PDB entry 3L24 and matched the resulting $2F_o - F_c$ density (Figure 3a,b).[18] Differences were observed in the side chains of the DPP between the two structures. However, these may appear to be minor and could be the result of either greater clarity based on the a higher resolution of the OPAA Y212F structure (2.4 Å) versus the previous 2.7 Å DPP bound wild-type OPAA structure, or alternative conformations of the ligand within the active site.

Global OPAA Insights Provided by the OPAA Y212F Structure. At the monomer level, OPAA Y212F largely mirrors the tertiary and secondary structure of the 440 residues visible in the wild-type OPAA structure (Figure 4a,b).[18] Only a few minor differences between secondary structures were noted when the Definition of Secondary Structure of Proteins software (DSSP) was applied to OPAA Y212F (Figure 4a). Surprisingly, the high degree of similarity at the secondary and tertiary levels did not extend to the expected quaternary structure. OPAA Y212F was found to be a dimer in the asymmetric unit with electron density being observed for the bulk of the 440 amino acids found in the expression construct. This dimeric arrangement of OPAA Y212 was not fully

DOI: 10.1021/acs.biochem.5b00624
Biochemistry 2015, 54, 6423−6433

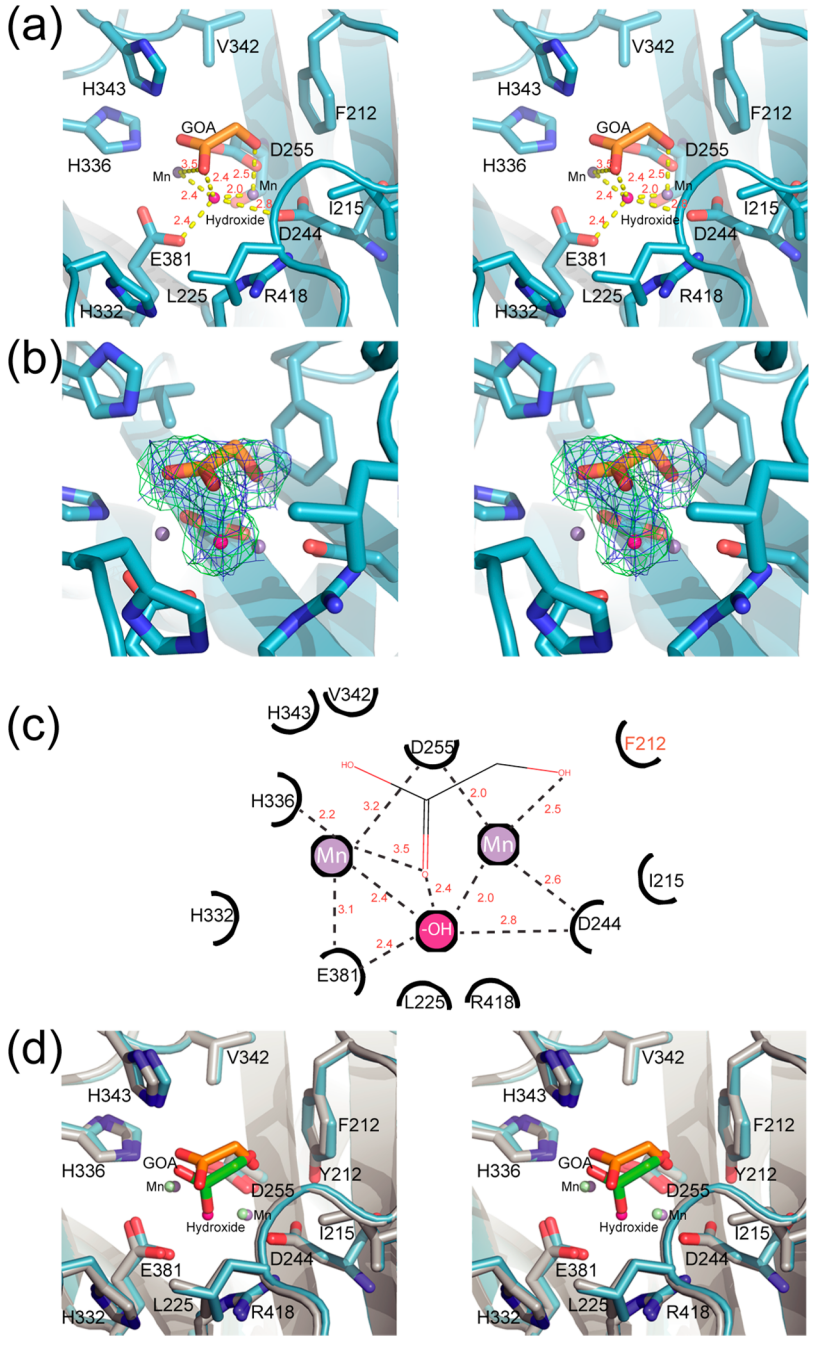

Figure 2. Comparison of the active sites of OPAA Y212F and wild-type OPAA. (a) Wall-eyed stereoview of the Y212F (krypton) active site bound to glycolate (GOA; orange) interacting with the binuclear Mn(II) (light purple) and hydroxide (hot pink). Red labels and dashed lines indicate distances measured in angstroms. The binuclear Mn(II) and hydroxide molecule are scaled down for the sake of clarity. (b) Wall-eyed stereoview of Y212F $F_o - F_c$ density (green mesh) from a simulated annealing omit map scaled to 2.5σ when refined in the absence of glycolate and hydroxide overlaid with Y212F $2F_o - F_c$ density scaled to 1σ (blue mesh). (c) Two-dimensional representation of the Y212F active site surrounding the bound glycolate. Residue labels and crescents in black represent the interactions of residues with glycolate, Mn(II), and hydroxide. The residue labeled in red represents the mutated residue, and dashed lines and red labels indicate distances measured in angstroms. (d) Wall-eyed stereoview of Y212F bound to glycolate interacting with binuclear Mn(II) and hydroxide colored as in panel a overlaid with wild-type OPAA (gray, PDB entry 3L24) bound with glycolate (green) and interacting with binuclear Mn(II) (light green) and hydroxide (hot pink).

unexpected. Previously, similar wild-type OPAA dimers were proposed within the wild-type OPAA crystal structure *I*222 lattice. Specifically, asymmetric unit monomers partnered with their lattice mates.[18,19] However, this is where the similarity ends. Previous examination of wild-type OPAA PDB entries 3L24 and 3L7G within their *I*222 crystal lattices had been used to support the idea that wild-type OPAA forms a dimer of dimers.[18,19] However, this type of arrangement is not found in the OPAA Y212F C2 crystal lattice, likely ruling out such a quaternary structural organization for at least OPAA Y212F (Figure 4c). To further probe the oligomer state of OPAA Y212F, and the wild-type variant OPAA and other associated OPAA mutants, they were run on a native gel. All proteins predominately migrated as a monomer (Figure S3).

DOI: 10.1021/acs.biochem.5b00624
Biochemistry 2015, 54, 6423−6433

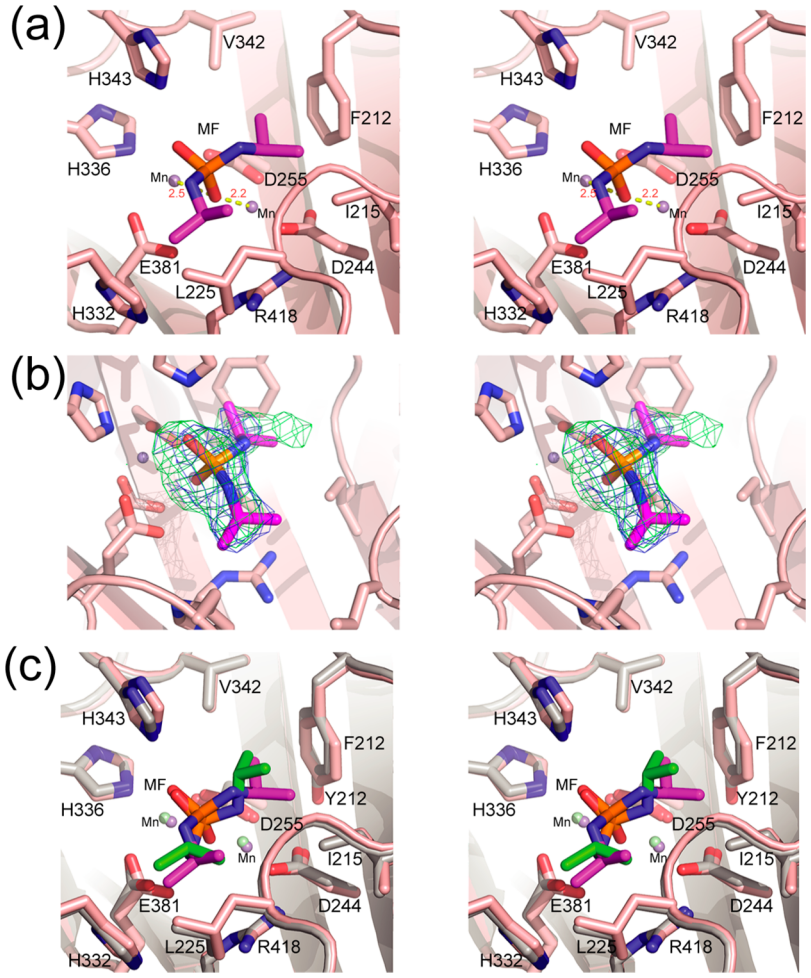

Figure 3. Comparison of the active sites of OPAA Y212F cocrystallized with mipafox and wild-type OPAA cocrystallized with mipafox. (a) Wall-eyed stereoview of the Y212F (light pink) active site bound to mipafox (purple) interacting with the binuclear Mn(II) (light purple). Red labels and dashed lines indicate distances measured in angstroms. The binuclear Mn(II) is scaled down for the sake of clarity. (b) Wall-eyed stereoview of Y212F cocrystallized with mipafox $F_o - F_c$ density (green mesh) from a simulated annealing omit map scaled to 2.5σ when refined in the absence of mipafox and hydroxide (green mesh) overlaid with Y122F cocrystallized with mipafox $2F_o - F_c$ density scaled to 1σ (blue mesh). (c) Wall-eyed stereoview of Y212F bound to mipafox interacting with binuclear Mn(II) colored as in panel a overlaid with the wild-type OPAA cocrystal (gray; PDB entry 3L7G) bound with mipafox (green) and interacting with binuclear Mn(II) (light green).

In addition to the lattice differences between OPAA Y212F and its wild-type counterpart, there were some notable differences in missing loops between the two. OPAA Y212F monomers A and B lacked electron density for residues 92−96 and 91−96, respectively, where this loop was observed in the wild-type OPAA structure. However, monomer B of OPAA Y212F was overall more complete than that observed for its monomer A but also surprisingly than those of any of the wild-type OPAA monomers. Specifically, electron density was observed for monomer B's residues 348−365. This newly resolved region includes reverse turns not observed in monomer A or in any of the three previously reported monomers found in the wild-type OPAA structure's asymmetric unit, giving it a handlelike appearance (Figure 3b and Figure S4).[18] Residues 351−354 form a type I reverse turn, whereas a type II reverse turn is formed by residues 360−363. Overall, this gives the newly resolved region a handlelike appearance. Lattice packing did not appear to be responsible for visualization of this additional tertiary structure, as this part of the structure is not directly in contact with other monomers, or symmetry mates.

A Second Round of Small Pocket Optimization Further Enhances OPAA Activity toward VR. Leveraging the improved activities of OPAA containing the Y212F and Y212V mutations, we then made two separate series of mutants in the OPAA Y212F and Y212V backgrounds, respectively. In each case, this involved substituting all amino acids at the nearby small pocket-forming Val342 site. Crude lysates from all these mutants were then used to screen for activity on 3 mM VR. None of the Val342 OPAA mutants constructed in the Y212V background showed VR activity increased over that of the parental Y212V strain (Figure S5); however, several of those from the Y212F background were of interest (Figure S6). In short, the crude lysates of the Y212F/V342C and Y212F/V342I OPAA mutants had specific activities ∼2 times that of the Y212F background, the OPAA Y212F/V342W and OPAA Y212F/V342Y lysates were ∼3 times as active as OPAA Y212F, and the OPAA Y212F/V342L construct was 7 times more active than OPAA Y212F (Figure 1 and Table 1). In short, mutants V342C, V342W, V342Y, and, in particular, V342L all appeared to have VR activity significantly increased over that of the parental Y212F. A closer kinetic examination using purified protein from the top performing OPAA Y212F/V342L mutant

DOI: 10.1021/acs.biochem.5b00624
Biochemistry 2015, 54, 6423−6433

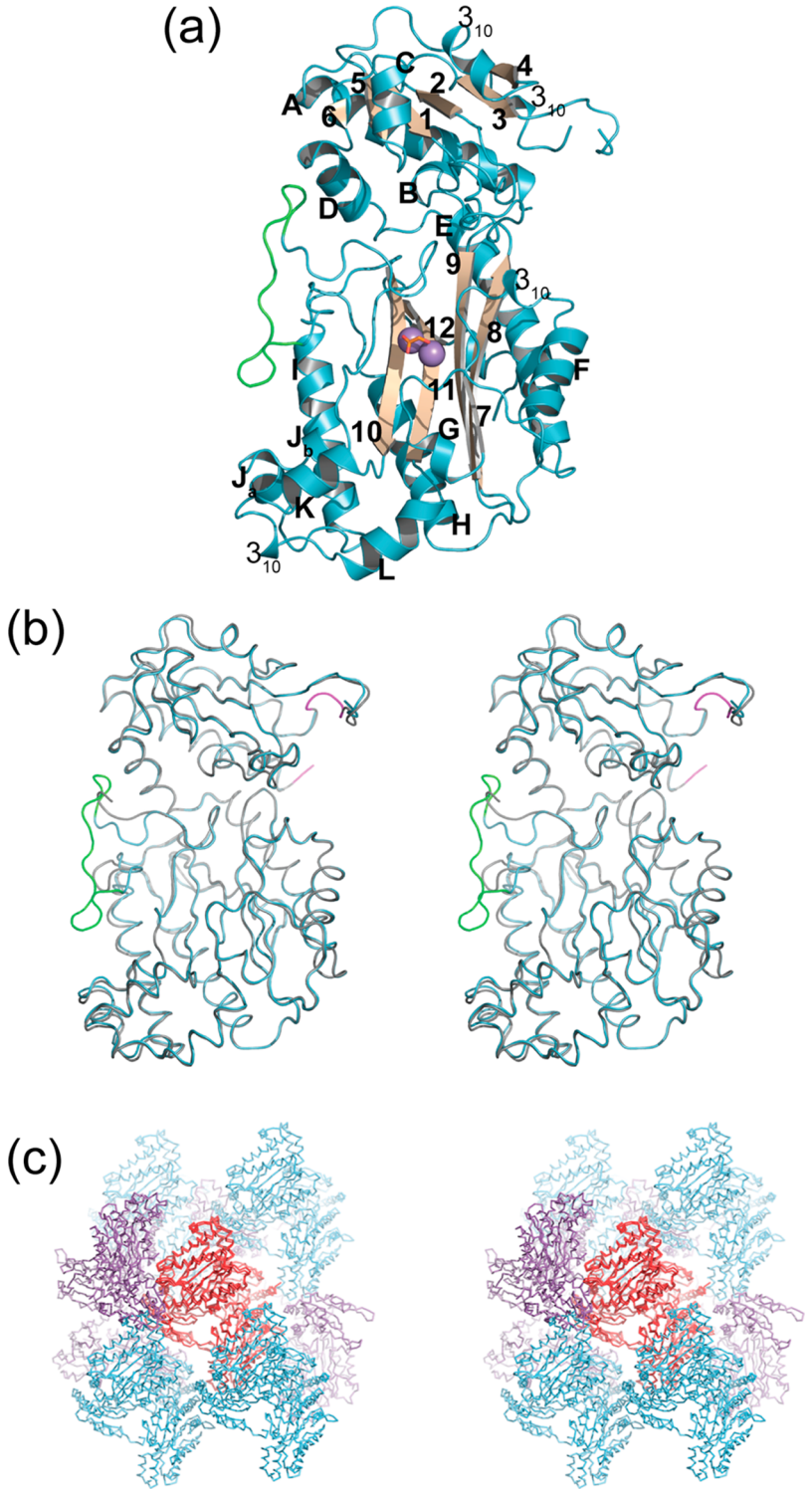

Figure 4. Tertiary and quaternary structure of OPAA Y212F. (a) Cartoon representation of the Y212F bound with glycolate (GOA; orange) and interacting with Mn(II) (light purple). Helical regions are colored krypton, identified using letters; β-sheets are colored wheat, identified using numbers, and the additional residues, which make the handle, are colored green. (b) Wall-eyed stereoview of the Y212F wire diagram showing the extra residues making the handle (green) and the missing residues (magenta). (c) Wall-eyed stereoview of the Y212F lattice (teal) overlaid with wild-type OPAA (purple; PDB entry 3L24). The monomer common to both lattices is colored red.

against VR revealed it possessed a k_{cat} for VR that was 2 times that of Y212F and 10 times higher than that of wild-type OPAA. When OPAA Y212F/V342L's slightly lower K_m for VR is taken into account, OPAA Y212F/V342L boasted 5- and 20-fold increased catalytic efficiency over that of OPAA Y212F and that of wild-type OPAA, respectively (Table 1 and Figure 1).

With a goal of further improvement in activity, the I215 site proved to be of interest because of its proximity to the small pocket. Consequently, all amino acids were substituted into the I215 site. Intriguingly, crude lysate specific activity screenings suggested that OPAA Y212F/V342L/I215Y (FLY) was the most active (Figure S7). In-depth analysis revealed its k_{cat} to be

DOI: 10.1021/acs.biochem.5b00624
Biochemistry 2015, 54, 6423−6433

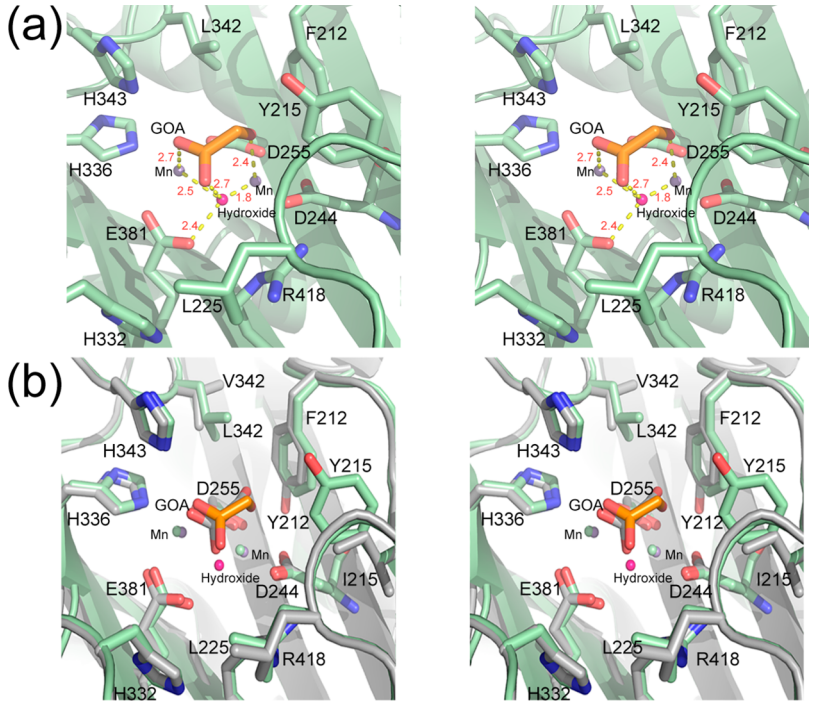

Figure 5. Comparison of the active sites of OPAA FLY and wild-type OPAA. (a) Wall-eyed stereoview of the FLY (light green) active site bound to glycolate (GOA; orange) interacting with the binuclear Mn(II) (light purple) and hydroxide (hot pink). Red labels and dashed lines indicate distances measured in angstroms. The binuclear Mn(II) and water are scaled down for the sake of clarity. (b) Wall-eyed stereoview of FLY bound to glycolate interacting with binuclear Mn(II) and hydroxide colored as in panel a overlaid with wild-type OPAA (gray; PDB entry 3L24) bound with glycolate (charcoal) and interacting with binuclear Mn(II) (light green) and hydroxide (hot pink).

2 times that of the double mutant OPAA Y212F/V342L, while its K_m toward VR was nearly unchanged (Figure 1 and Table 1). Crude lysate data also suggested OPAA Y212F/V342L/I215H and OPAA Y212F/V342L/I215F were of interest but were not as active as the OPAA FLY.

To evaluate the alterations occurring within the OPAA active site due to the triple mutation, the X-ray structure of OPAA FLY was determined to 2.4 Å using methods identical to those used for the OPAA Y212F structure. With its structure being determinied in the same space group and lattice, OPAA FLY at the quaternary, tertiary, and secondary structure levels closely resembled OPAA Y212F (data not shown). Even the additional active site density mirrored the glycolate and the metal bridging hydroxide ion previously observed in the OPAA Y212F structure (Figure 5). Apart from the Y212F, V342L, and I215F alterations, only minor differences between the OPAA FLY and other OPAA structures were observed.

Broadened Stereospecificity of OPAA FLYD. An enzyme's enantiomeric preference, where it exists, can be determined by degrading half the substrate (essentially, the enantiomer on which the activity is greatest) and measuring the direction in which the remaining substrate (i.e., the least preferred enantiomer) rotates plane polarized light in a polarimeter. Following that approach, the PTE enzyme was used to degrade a solution of 1 g of VR in 1 L of buffer. The reaction mixture was sampled periodically; the reaction was followed spectrophotometrically, and the mixture was extracted with ethyl acetate when just more than half the starting VR had been degraded. The concentrated ethyl acetate extract of that solution was determined by polarimetry to be comprised predominantly of the P(−) enantiomer, indicating an enzymatic preference for the P(+) enantiomer.

Using knowledge of the enantiomeric preference of one enzyme on one substrate, it is possible to mix that reference enzyme with one of unknown enantiomeric preference at similar activity levels and observe whether their respective preferences are for the same or for different enantiomers of that substrate. If two enzymes prefer the same enantiomer, one enantiomer will not be degraded and the hydrolysis reaction curve will have a midpoint deflection similar to that observed with a single enzyme that strongly prefers one enantiomer. If the two enzymes prefer different enantiomers such that the activity of one enzyme complements the activity of the other, no such midpoint deflection will be observed, resulting in a typical single-exponential curve. Using this approach, we determined that the OPAA WT enzyme possessed the same enantiomeric preference as PTE; i.e., it preferentially catalyzed the P(+) enantiomer.

Figure 6 shows the patterns of OPAA wild-type, F, FL, and FLY enzymes on 0.18 mM VR. The concentration of VR was selected to allow a complete reaction within the dynamic range of the spectrophotometer. Clearly, the wild-type enzyme and the F, FL, and FLY mutant OPAA enzymes all exhibit an almost absolute specificity for a single enantiomer of VR, as evidenced by the relatively rapid initial rate followed by an abrupt midpoint deflection to a rate approximating that of spontaneous VR hydrolysis.

Studying the OPAA Y212F active site with mipafox bound as well as the OPAA FLY active site, we conducted a search for residues to be targeted for mutation to broaden the stereospecificity of OPAA FLY. Of the ones considered, His343 was of particular interest. It was the lone residue not optimized within the small pocket, and it formed an H-bond with an oxygen atom with the diamidophosphate core potentially orienting the bound ligand. Two mutants were

DOI: 10.1021/acs.biochem.5b00624
Biochemistry 2015, 54, 6423−6433

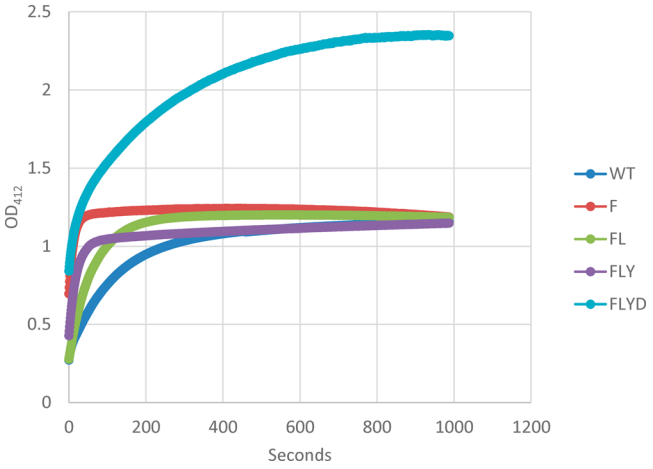

Figure 6. Reaction profiles of wild-type, F, FL, FLY, and FLYD enzymes on 0.18 mM VR. WT, F, FL, and FLY catalyze a single enantiomer, while FLYD catalyzes both enantiomers of VR. Enzyme concentrations were as follows: 1.4 mg/mL WT, 2.75 mg/mL F, 0.6 mg/mL FL, 0.62 mg/mL FLY, and 1.75 mg/mL FLYD.

constructed at the His343 site, H343D and H343A. One, H343D, exhibited activity toward both enantiomers of VR. This mutant, designated OPAA FLYD, illustrated a relatively constant rate for the entire reaction with a final magnitude twice that of the others, indicative of OPAA FLYD having similar activity on both enantiomers of VR. Overall, kinetic analysis of OPAA FLYD revealed it possesses a k_{cat} of 18 min^{-1}, while its VR K_m was 2075 μM on racemic VR, equating to a catalytic efficiency of 8890 M^{-1} min^{-1}, or approximately half that of FLY. This translates into OPAA FLYD possessing a 16-fold increase in catalytic efficiency over that of the wild-type enzyme, and more importantly possessing a substantially broader stereospecificity for VR, as compared to those of previous versions of the enzyme (Figure 6).

DISCUSSION

Insight into the Participation of Hydroxide in the OPAA Catalytic Mechanism. Unlike the amidohydrolase superfamily of phosphotriesterases (PTEs) in which a number of X-ray structures have been determined and support their proposed catalytic mechanism, structural information about OPAA is relatively scarce. Most of the information pertaining to the OPAA catalytic mechanism has been derived from studies of an enzyme structurally similar to OPAA known as aminopeptidase P (AMPP).[5,20] The currently envisioned mechanism for OPAA has a substrate entering the substrate-binding site and displacing waters bound to the manganese(II) ions. Subsequently, hydroxide bridging between two manganese(II) ions has been proposed to perform a nucleophilic attack on the phosphorus center of the substrate in question, triggering the formation of an intermediate. This intermediate subsequently collapses with the departure of the leaving group.[5] Regrettably, in the only two previously known structures of OPAA, the hydroxide ion at the center of the proposed mechanism has been difficult to fully confirm.[18] However, within the OPAA Y212F and FLY structures, clear density is observed because of the presence of a hydroxide ion being bridged by the two manganese(II) ions (Figure 2b). In an earlier study, an aspartic acid within the PTE family of enzymes was shown to form a hydrogen bond with the hydroxide ion priming it for its role in catalysis.[5] The placement of the hydroxide within the OPAA Y212F and FLY structures directly implicates Glu381 to fill this role for OPAAs. In addition to coordinating one of the two manganese(II) ions within the OPAA active site, Glu381 is in a prime location and orientation to form the requisite hydrogen bond (Figure 2a,b).

Increase in OPAA Activity toward VR through Small Pocket Optimization. With the larger side chain moieties of the V-series agents compared to those of the G-series, a first-glance assumption might be that increasing the size of the substrate-binding site would facilitate greater OPAA activity toward the larger organophosphates such as the V-series agents, including VR. However, it is not that straightforward. In actuality, the mutational screening data suggest that the plasticity of certain parts of the small pocket, a shifted H-bonding network, and its shape are the predominate influences for the increased activity toward VR.

For instance at the Y212 site, substitutions that would likely have disrupted a hydrogen bonding network tying the upper part of the small pocket to manganese(II) coordinating Asp255 seemed to be favored. In general, residues at this location that likely would not hamper hydrophobic interactions or create steric clashes with nearby Val342 also appear to be better substitutes (Figure S2). Interestingly, the mutational data for the 342 site appear to attest to desirable nature of a hydrophobic connection between sites 342 and 212 for heightened OPAA VR capability. Specifically, the substitution of leucine at site 342 appears to balance an increasing number of hydrophobic interactions with the substituted phenylalanine at position 212 without creating steric clashes (Figure S6). Altogether, the stronger hydrophobic interactions along the wall of the small pocket, while increasing the plasticity of the wall relative to the manganese(II) active site core, appear to be beneficial for VR catalysis.

However, the additional plasticity resulting from the Y212F mutation may not be the only factor in the increased rate of catalysis of the Y212F OPAA mutant. The presence of the hydroxide ion within the structures of the Y212F and FLY OPAAs and not in the wild-type OPAA might offer an additional clue. Specifically, the loss of the H-bonds formed by the replacement of tyrosine with phenylalanine at position 212 alters the H-bonding network in a manner that allows for more stable interactions between the active site hydroxide ion and neighboring residues. One possible candidate would be D244. Whereas D244 forms H-bonds with Y212 in wild-type OPAA, these interactions are no longer available for D244 in Y212F OPAA and subsequent Y212F mutation-containing mutants. This could translate into D244 being more available to facilitate interactions with the observed active site hydroxide ion that is only 2.8 Å away and stabilize its presence. This stabilizing effect on the hydroxide ion by D244 or other active site residues as a result of the Y212F mutation-containing OPAA mutants could in turn heighten catalytic activity within the proposed enzymatic mechanism.[5]

In addition to these factors and contrary to initial assumptions, shrinking the small pocket appears to also be beneficial for catalysis of VR. As the screening data illustrate, significant relative increases in activity toward VR were found when Ile215 was exchanged with residues possessing bulkier side chains. These substitutes narrow the size of the small pocket significantly (Figure 7). With little unchanged outside of the sites that were mutated within the OPAA substrate-binding site and accompanying manganese(II) ion core, the narrowing of the active site appears to suggest the narrower small pocket

DOI: 10.1021/acs.biochem.5b00624
Biochemistry 2015, 54, 6423−6433

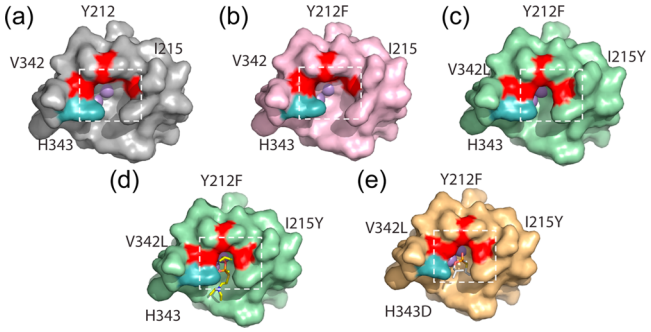

Figure 7. Surface area of wild-type OPAA with mipafox, Y212F with mipafox, and FLY substrate-binding sites. (a) Surface area representation of the substrate-biding sites for wild-type OPAA cocrystallized with mipafox (gray; PDB entry 3L7G), (b) Y212F cocrystallized with mipafox (light pink), and (c) FLY (light green). (d) Same as panel c with the placement of the VR P(+) enantiomer in the active site. (e) Model of FLYD based on the FLY (light brown) active site with alteration of H343D and placement of a VR P(−) enantiomer in the active site. The substrate-binding site in all panes is outlined in the white box, and the amino acids sites, 212, 342, and 215, are colored red, with H343 colored dark teal. Mipafox in panels a and b was removed for the sake of clarity of the small pocket space. Active site manganese ions are shown as light purple spheres.

could restrict VR to an orientation more favorable for catalysis. Understandably, without a structure of VR within the OPAA FLY active site, determining the exact effect on VR positioning by the narrowing of the small pocket for the increase in OPAA catalytic activity toward VR as a result of the narrowing of the small pocket is difficult. However, small changes in orientation of substrates due to mutations away from the active site have been observed to result in large catalytic differences, and this may be the case for OPAA and VR.[21]

Broadening Stereospecificity of OPAAs. With differing levels of toxicity known between enantiomers of organophosphates, enzymes that can process either the more toxic enantiomer or both enantiomers of a given organophosphate would be strongly preferred for therapeutic use. Using the DPP-bound OPAA Tyr212 and wild-type structures as a guide, three points of contact within the substrate-binding site are readily highlighted as contributing to OPAA's substrate stereospecificity. Two are based on favorable interactions between the DPP side chains and the small and large pockets. One other could be located with interactions with DPP's diamidophosphate core and the enzyme's binuclear metal core.

Beyond these points of contact, a fourth is likely present in the form of a H-bond between $N_{\varepsilon 2}$ of the His343 side chain and an oxygen atom from the diamidophosphate core. In recent reports, His343 has been suggested to assist in polarization of scissile peptide carbonyl bonds within naturally occurring peptide substrates.[18] With regard to organophosphates, the previously proposed catalytic mechanism suggested His343 could assist in positioning them for catalysis.[5] Although this seems straightforward for the binding and catalysis of several organophosphate classes, including V-series agents for their respective P(+) enantiomers, the bulky side chain of His343 might sterically hinder P(−) enantiomers from accessing the active site in a catalytically viable manner (Figure 7d,e). As a result, the broadened activity observed at the expense of some catalytic efficiency in the OPAA FLYD mutant could be rationalized by the removal of the steric hindrance H343 poses toward P(−) enantiomers. Other substitutions at the H343 site have not yet been investigated.

Naturally, this alteration of His343 may dampen some catalytic activity of one enantiomer over another. However, broader substrate activity, along with a 16-fold increase in catalytic activity toward VR, is quite a boon toward considering OPAAs in the role of catalytic antidotes. Combined with the high levels of expression, stability, and high GD activity inherent to this enzyme, the OPAA FLY and FLYD mutants appear to offer potentially suitable platforms for further modifications aimed at increasing the catalytic efficiency of this enzyme on VR.

■ ASSOCIATED CONTENT

Supporting Information

The Supporting Information is available free of charge on the ACS Publications website at DOI: 10.1021/acs.biochem.5b00624.

Mutant screening data for OPAA sites Y292, Y212, V342, and I215 as well as density maps of residues 348−365 (Figures S1−S7) (PDF)

Accession Codes

The atomic coordinates and structure factors have been deposited with the Brookhaven Protein Data Bank as entries 4ZWO, 4ZWP, and 4ZWU.

■ AUTHOR INFORMATION

Corresponding Authors

*College of Pharmacy, University of Georgia, 422 Pharmacy South, Athens, GA 30602, or U.S. Army Edgewood Chemical Biological Center, Aberdeen Proving Ground, MD 21010-5424. E-mail: spegan@uga.edu. Telephone: (706) 542 3435.

*E-mail: steven.p.harvey6.civ@mail.mil. Telephone: (410) 436-8646.

Funding

This research was supported by funds made available by the Defense Threat Reduction Agency CB3742 (S.P.H.). Use of the Advanced Photon Source was supported by the U.S. Department of Energy, Office of Science, Office of Basic Energy Sciences, under Contract W-31-109-Eng-38 (S.D.P.).

Notes

The authors declare the following competing financial interest(s): A provisional U.S. Patent Application 62/171,727 has been filed to cover the developed enzyme.

■ ABBREVIATIONS

ALS, Advanced Light Source; AMPP, aminopeptidase P; CASARM, Chemical Agent Standard Analytical Reference Material; DDFP, *N*,*N*′-diisopropyldiamidofluorophosphate; DDP, *N*,*N*′-diisopropyldiamidophosphate; DFP, diisopropylfluorophosphate; DSSP, Definition of Secondary Structure of Proteins; DTNB, 5,5′-dithiobis(2-nitrobenzoic acid); GOA, glycolate; OPAA, organophosphorus acid anhydrolase; OPAA FLY, Y212F/V342L/I215Y; 2-PAM, poisoned acetylcholinesterase; PISA, Proteins, Interfaces, Structures and Assemblies; PON1, phosphotriesterase; PTE, phosphotriesterase; Soman, *o*-pinacolyl methylphosphonofluoridate; VR, Russian VX, *O*-isobutyl *S*-[2-(diethylamino)ethyl] methylphosphonothioate; VX, *O*-ethyl *S*-[2-(diisopropylamino)ethyl] methylphosphonothioate.

DOI: 10.1021/acs.biochem.5b00624
Biochemistry 2015, 54, 6423−6433

REFERENCES

(1) Eddleston, M. (2000) Patterns and problems of deliberate self-poisoning in the developing world. *QJM: monthly journal of the Association of Physicians 93*, 715−731.

(2) Phillips, M. R., Li, X., and Zhang, Y. (2002) Suicide rates in China, 1995−99. *Lancet 359*, 835−840.

(3) Buckley, N. A., Roberts, D., and Eddleston, M. (2004) Overcoming apathy in research on organophosphate poisoning. *BMJ 329*, 1231−1233.

(4) Petrikovics, I., Cheng, T. C., Papahadjopoulos, D., Hong, K., Yin, R., DeFrank, J. J., Jaing, J., Song, Z. H., McGuinn, W. D., Sylvester, D., Pei, L., Madec, J., Tamulinas, C., Jaszberenyi, J. C., Barcza, T., and Way, J. L. (2000) Long circulating liposomes encapsulating organophosphorus acid anhydrolase in diisopropylfluorophosphate antagonism. *Toxicol. Sci. 57*, 16−21.

(5) Bigley, A. N., and Raushel, F. M. (2013) Catalytic mechanisms for phosphotriesterases. *Biochim. Biophys. Acta, Proteins Proteomics 1834*, 443−453.

(6) Cheng, T., Liu, L., Wang, B., Wu, J., DeFrank, J. J., Anderson, D. M., Rastogi, V. K., and Hamilton, A. B. (1997) Nucleotide sequence of a gene encoding an organophosphorus nerve agent degrading enzyme from Alteromonas haloplanktis. *J. Ind. Microbiol. Biotechnol. 18*, 49−55.

(7) DeFrank, J. J., Beaudry, W. T., Cheng, T. C., Harvey, S. P., Stroup, A. N., and Szafraniec, L. L. (1993) Screening of halophilic bacteria and Alteromonas species for organophosphorus hydrolyzing enzyme activity. *Chem.-Biol. Interact. 87*, 141−148.

(8) DeFrank, J. J., and Cheng, T. C. (1991) Purification and properties of an organophosphorus acid anhydrase from a halophilic bacterial isolate. *Journal of bacteriology 173*, 1938−1943.

(9) Benschop, H. P., Konings, C. A., Van Genderen, J., and De Jong, L. P. (1984) Isolation, anticholinesterase properties, and acute toxicity in mice of the four stereoisomers of the nerve agent soman. *Toxicol. Appl. Pharmacol. 72*, 61−74.

(10) Tsai, P. C., Fox, N., Bigley, A. N., Harvey, S. P., Barondeau, D. P., and Raushel, F. M. (2012) Enzymes for the homeland defense: optimizing phosphotriesterase for the hydrolysis of organophosphate nerve agents. *Biochemistry 51*, 6463−6475.

(11) Hall, C. R., Inch, T. D., Inns, R. H., Muir, A. W., Sellers, D. J., and Smith, A. P. (1977) Differences between some biological properties of enantiomers of alkyl S-alkyl methylphosphonothioates. *J. Pharm. Pharmacol. 29*, 574−576.

(12) Kuca, K., Jun, D., Cabal, J., Hrabinova, M., Bartosova, L., and Opletalova, V. (2006) Russian VX: inhibition and reactivation of acetylcholinesterase compared with VX agent. *Basic Clin. Pharmacol. Toxicol. 98*, 389−394.

(13) Cheng, T. C., Harvey, S. P., and Chen, G. L. (1996) Cloning and expression of a gene encoding a bacterial enzyme for decontamination of organophosphorus nerve agents and nucleotide sequence of the enzyme. *Applied and environmental microbiology 62*, 1636−1641.

(14) Otwinowski, Z., and Minor, W. (1997) *Processing of X-ray Diffraction Data Collected in Oscillation Mode*, Vol. *276*, Macromolecular Crystallography, Part A, Academic Press, New York.

(15) Collaborative Computational Project, Number 4 (1994) The Ccp4 Suite - Programs for Protein Crystallography. *Acta Crystallogr., Sect. D: Biol. Crystallogr. 50*, 760−763.

(16) Adams, P. D., Afonine, P. V., Bunkoczi, G., Chen, V. B., Davis, I. W., Echols, N., Headd, J. J., Hung, L. W., Kapral, G. J., Grosse-Kunstleve, R. W., McCoy, A. J., Moriarty, N. W., Oeffner, R., Read, R. J., Richardson, D. C., Richardson, J. S., Terwilliger, T. C., and Zwart, P. H. (2010) PHENIX: a comprehensive Python-based system for macromolecular structure solution. *Acta Crystallogr., Sect. D: Biol. Crystallogr. 66*, 213−221.

(17) Emsley, P., and Cowtan, K. (2004) Coot: model-building tools for molecular graphics. *Acta Crystallogr., Sect. D: Biol. Crystallogr. 60*, 2126−2132.

(18) Vyas, N. K., Nickitenko, A., Rastogi, V. K., Shah, S. S., and Quiocho, F. A. (2010) Structural insights into the dual activities of the nerve agent degrading organophosphate anhydrolase/prolidase. *Biochemistry 49*, 547−559.

(19) Vyas, N. K., Nickitenko, A., Rastogi, V. K., Shah, S. S., and Quiocho, F. A. (2010) Correction to Structural insights into the dual activities of the nerve agent degrading organophosphate anhydrolase/prolidase. *Biochemistry 49*, 2305−2305.

(20) Huang, L. F., Su, B., Jao, S. C., Liu, K. T., and Li, W. S. (2006) Aminopeptidase p mediated detoxification of organophosphonate analogues of sarin: mechanistic and stereochemical study at the phosphorus atom of the substrate. *ChemBioChem 7*, 506−514.

(21) Mesecar, A. D., Stoddard, B. L., and Koshland, D. E., Jr. (1997) Orbital steering in the catalytic power of enzymes: small structural changes with large catalytic consequences. *Science 277*, 202−206.

DOI: 10.1021/acs.biochem.5b00624
Biochemistry 2015, 54, 6423−6433